An embedded crack in a constant strain triangle utilizing extended finite element concepts

Olesen, J.F.; Poulsen, P.N.

Published in:
Computers & Structures

Link to article, DOI:
10.1016/j.compstruc.2012.11.006

Publication date:
2013

An embedded crack in a constant strain triangle utilizing extended finite element concepts

J.F. Olesen*, P.N. Poulsen

Department of Civil Engineering, Technical University of Denmark, Brovej 118, DK-2800 Kgs. Lyngby, Denmark

Abstract

This paper revisits the formulation of the CST element with an embedded discrete crack taking advantage of the direct formulations developed within the framework of the extended finite element method, XFEM. The result is a simple element for modeling cohesive fracture processes in quasi-brittle materials. The element is easily fitted a standard FEM code, and as such it is an alternative to more cumbersome XFEM elements which require special d.o.f.'s and extra administration. The crack description is embedded, in the sense that extra d.o.f.'s controlling the crack opening are eliminated at the element level. The cracked element is stress-compatible in the sense that stresses are continuous across the crack. A special shape function is introduced to allow for the discontinuous displacements without eradicating the stress compatibility. The simplicity of the element comes at the cost of inter-element discontinuity of displacements. The formulation is based on a variational principle of virtual work involving only the interpolation of displacements. The good performance of the element is demonstrated through the comparison with three benchmark tests in which a single crack is propagated: The center cracked sheet in uni-axial tension, the three-point bending test and the four-point shear beam test.

Keywords: Fracture mechanics, discrete crack modeling, cohesive crack, embedded crack

*Corresponding author
Email address: jfo@byg.dtu.dk (J.F. Olesen)

1. Introduction

The detailed modeling of reinforced concrete structures under service life conditions as well as in the ultimate limiting states is a challenging task encompassing not only the modeling of fracture propagation, multiple cracks and crossing cracks but also the constitutive behavior of cracks. The pursuit of this aim is promoted by the need for more reliable descriptions of the mechanical performance in the cracked state. Here we mention the need for better description of the development of structural stiffness, the influence of cyclic loading, stability and vibrations. Further, there is a need for enhanced predictions of crack morphology, for the better understanding of deteriorating processes in particular, and for more precise estimates of service life in general.

The numerical modeling of fracture processes in quasi-brittle materials started with the pioneering paper by Hillerborg et al. in 1976 [1]. This work was the first to present the ground breaking *fictitious crack model* for the modeling of cohesive fracture propagation in quasi brittle materials. Early attempts to model crack propagation were based on interface elements placed at the predefined crack path. Later, the modeling of fracture propagation within finite elements evolved from methods for handling weak discontinuities over embedded strong discontinuities applying multi-field variational principles, into the powerful method known as the eXtended Finite Element Method (XFEM), see [2] and [3]. Recently, other methods for the modeling of strong discontinuities have emerged namely the meshless methods, see e.g. Rabczuk et al. [4].

Since the introduction of XFEM by Belytschko and Black [2] and Moës et al. [3] it has proven itself to be a strong tool for modeling discrete cracks. XFEM has the ability to independently model the separated parts of the element without any coupling, which is the reason for its unique modeling capabilities, see e.g. [5]. XFEM was introduced for linear elastic fracture mechanics but has since been applied to cohesive crack modeling, see e.g. [6], [7] and [8]. Modeling of three-dimensional crack propagation has also been performed, see e.g. Areias and Belytschko [9]. In recent years partly cracked elements have been formulated, the first by Zi and Belytschko [10]. Lately, formulations with additional parameters in the enrichment have been presented by Asferg et al. [11] and Mougaard et al. [12]. In the latest developments by Mougaard et al. [12] reasonable accuracy is obtained with coarse element meshes, e.g. the standard three point bending test may be modeled

using elements with a characteristic side length as large as one fourth of the height of the beam, see [12]. An alternative enrichment strategy has been developed by Karihaloo and Xiao [13] applying exact asymptotic displacement fields obtained for many commonly used cohesive laws. This enrichment is potentially accurate; however, it does not comply with the concept of element local shape functions applied in FEM. The undoubtedly good performance of XFEM in modeling discrete crack growth has the drawback of cumbersome administration e.g. from ensuring conformity at the boundary of enhanced elements, see [12], and additional computational costs due to extra degrees of freedom at the system level. In view of the complexities and costs of XFEM simpler alternatives might be appealing.

The objective of the present work is to take advantage of XFEM achievements, however, without accepting extra parameters at the system level. This implies the need for elimination of such parameters at the element level. The means for this elimination is the requirement of traction continuity across the crack, and the result is an embedded solution. A comparative study of the performance of the embedded approach versus XFEM is reported in [17] where it is shown that there is no great difference in the accuracy of the two methods.

Here the aim is to formulate a CST element with an embedded discrete crack taking advantage of the direct formulations developed within the framework of XFEM. This straightforward formulation is based on a variational principle of virtual work involving only the interpolation of displacements. Now, the CST element is capable of modeling constant strains which in a linear elastic continuum result in constant stresses. In a standard XFEM formulation the CST element is enriched by 6 d.o.f.'s in order to allow for a separation of the element in two independent continua, see [15]. The result is a model with a linearly varying opening and sliding; and with an inerratic stress-crack opening relation, an approximately linear variation of the traction across the crack is obtained. This linear variation is not compatible with the stresses in a basic CST element. However, a discontinuous CST element with a constant opening and sliding, and thereby a constant traction across the crack, would be compatible with the basic CST element. A constant opening or sliding may be obtained by the use of a shape function which is a special subset of the standard discontinuous shape functions in XFEM for a CST element. The consequence of only making use of a subset of XFEM shape functions is that, as opposed to XFEM, we no longer have a full kinematic decoupling of the element parts separated by the crack. The

applied shape function has a constant opening, and models constant and equal strains/stresses on both sides of the crack and it vanishes on the side not cut by the crack and at the opposite node. The capability of modeling a constant opening and sliding requires two extra deformation parameters, however, these extra parameters are eliminated locally by demanding traction continuity in a strong form. The present formulation is based directly on the principle of virtual work, involving only the interpolation of deformations, and the result is a CST element which may embed a strong discontinuity. With the present model we restrict ourselves to the case where there is traction continuity across the crack, as is the case for cohesive cracks.

In [16] Jirásek classifies the different formulations of embedded discontinuities published before the turn of the century. This systematic work is based on a three-field Hu-Washizu variational form. From the perspective of [16], the present formulation is both statically and kinematically optimal, and it furnishes a symmetric incremental relationship. The reason being that both displacement fields and strain fields are enriched in the present formulation, and that strains are derived from displacements and that stresses are derived from strains.

Oliver [17], Feist et al. [18] and Linder et al. [19] all present a similar shape function to the one applied here, however, in these works the stress continuity across the crack is stated in the weak form. Moreover, in [17] the mathematical representation of the shape function implied the use of the Dirac delta function; and to get around the obstacle of dealing with delta functions a regularization via delta-sequences and a regularization parameter was introduced. In the present work there is no need for such regularization efforts due to the application of a XFEM type shape function. Further, it should be emphasized that, the variational method by Oliver [17], by the weak imposition of the traction continuity condition, belongs to the family of the assumed enhanced strain methods [20]; while the approach by Feist et al. is based on a three-field variational formulation. Linder et al. [19] arrive at the same shape function, via a similar approach to the one by Oliver [17], however, through a general approach covering quadrilaterals as well as triangles. Furthermore, their approach also belongs to the enhanced strain methods, although the enhanced parameters are constructed by imposing local equilibrium between stresses in the bulk of the element and the tractions on the crack face, and subsequently eliminated by static condensation at the element level. The present approach, however, is based on a variational formulation in terms of the virtual work equation, involving only the

interpolation of displacements like in XFEM, and thus, distinguishes itself from the methods based on a multi-field variational principle.

Dvorkin et al. [21] and Sancho et al. [22] present similar approaches to the present since they also eliminate extra d.o.f.'s based on traction continuity at the element level. The formulation by Dvorkin et al. was the first to present embedded localization lines. In this early contribution the displacement jump was established in quadrilaterals as a modification of the nodal degrees of freedom applying the standard shape functions. This is in contrast to XFEM where specific discontinuous shape functions are applied. Sancho et al. present a special triangular element where the discontinuity is restricted such that it must be parallel to an element side and located at mid-height.

The cost of the simplicity of the element presented here is an inherent lack of inter-element conformity. The piecewise constant approximation of the crack opening will lead to discontinuity in the crack opening between elements and incompatibility along the element edges that the crack intersects. It should be emphasized that the inter-element discontinuities are not accounted for in the variational formulation. However, since the inter-element jump in crack opening will decrease with mesh refinement, these incompatibilities will decrease, too. Further, the inter-element discontinuities are restrained through the interaction of common element side nodes. Thus, the inter-element non-conformity will not undermine the performance of the element. No formal proof of convergence is offered but good performance for coarse meshes and enhanced performance with mesh refinement is demonstrated through the three application examples.

The above mentioned costs of the simplicity of the element should be viewed in the light of the potential for further development of the element. Thus, it is foreseen that the present description will lend itself to a straightforward implementation of partly cracked stages and crossing cracks. This is especially interesting when pursuing the detailed description of the mechanical behavior of real life reinforced concrete structures exhibiting a multitude of intersecting and branching crack paths. However, this is beyond the scope of the present paper and will not be addressed any further.

Although earlier formulations of the embedded crack in a CST element in principle may be shown to embrace the present, the justification for this presentation is the novel direct approach to the formulation as well as the fact that it proves feasible and that it produces accurate results with rather coarse meshes compared to previously reported results in literature obtained

with XFEM.

2. Kinematics

The concepts of the extended finite element method for the approximation of a displacement field with a strong discontinuity is adopted here. Thus, the displacement field approximation in an element with a discontinuity is established by combining the displacement field corresponding to the continuous element with the displacement field corresponding to the discontinuity. For the linear interpolation of the continuous displacement field we consider a three-node triangular element, the CST. The element is given the possibility of a strong discontinuity along a straight line traversing the element.

We seek stress compatibility between the stresses in the continuous parts of the element and the stress vector bridging the discontinuity line. This is obtained in two steps: by making a proper choice for the discontinuous shape function, and by enforcing the traction on the crack faces to equal the bridging stresses due to the cohesive crack properties of the material. This is in contrast to other embedded methods and to XFEM where traction continuity is only obtained in the weak sense.

The proper choice of a discontinuous shape function is ensured by demanding that the order of variation of the discontinuous displacement fields along the discontinuity line must match the order of variation of the continuous stress fields, and that the discontinuous displacement field produces equal stresses on opposite sides of the discontinuity. In the case of a CST this leads to a displacement field with a constant jump in the displacement along the discontinuity line, which will produce constant bridging stresses along the discontinuity matching the constant stress field of the CST. Further, this displacement field must produce equal displacement gradients on either side of the discontinuity. A shape function which allows for a constant jump along a straight line and at the same time only introduces equal and constant displacement gradients on either side of the discontinuity line is shown in Figure 1. The shape function may be written in terms of the area coordinate associated with the element vertex which belongs to the sub-domain Ω_e^- as shown in the figure:

$$N_d = \begin{cases} \zeta - 1 & \text{in} \quad \Omega_e^- \\ \\ \zeta & \text{in} \quad \Omega_e^+ \end{cases} \tag{1}$$

Since the crack opening is constant along the crack in the element it may be described by a single crack opening vector, the jump vector. In the global (x_1, x_2)-coordinate system the jump vector is denoted by $\mathbf{V}_d$. Thus, the discontinuous deformation field vector $\mathbf{u}_d$ may now be introduced as

$$\mathbf{u}_d = \mathbf{N}_d \mathbf{V}_d = \begin{bmatrix} N_d & 0 \\ 0 & N_d \end{bmatrix} \begin{Bmatrix} V_1^d \\ V_2^d \end{Bmatrix} \tag{2}$$

whereby the total deformation field vector, $\mathbf{u}$, may be established as the combination of the continuous part, $\mathbf{u}_c$, and the discontinuous part:

$$\mathbf{u} = \mathbf{u}_c + \mathbf{u}_d = \mathbf{N}_c \mathbf{V}_c + \mathbf{N}_d \mathbf{V}_d \tag{3}$$

where $\mathbf{u}_c = \mathbf{N}_c \mathbf{V}_c$ is the standard CST displacement interpolation relationship.

Adopting the Voigt notation and assuming a linear strain measure, the strains in the continuous part of the element may be written as the vector

$$\boldsymbol{\epsilon} = \boldsymbol{\epsilon}_c + \boldsymbol{\epsilon}_d = \mathbf{B}_c \mathbf{V}_c + \mathbf{B}_d \mathbf{V}_d = \mathbf{B} \begin{Bmatrix} \mathbf{V}_c \\ \mathbf{V}_d \end{Bmatrix} \tag{4}$$

Here the right most equality defines the total strain interpolation matrix $\mathbf{B}$, where the first component $\mathbf{B}_c$ is the usual constant strain interpolation matrix and the second component $\mathbf{B}_d$ is the constant strain interpolation matrix derived from the discontinuous shape function. Note that $\mathbf{B}_d$ is the same on both sides of the discontinuity, and thus, there is no need to distinguish between the two sub-domains.

The jump vector referred to the local crack coordinate system is given by $[\![\mathbf{u}]\!] = [u_n \; u_s]^T$. Here u_n and u_s are the normal opening and tangential sliding of the crack faces, respectively, corresponding to the local (n, s)-coordinate system defined by the crack, see Figure 1. The relationship between local and global jump vectors is

$$[\![\mathbf{u}]\!] = \mathbf{T}_{cr} \mathbf{V}_d \tag{5}$$

where $\mathbf{T}_{cr}$ is the coordinate transformation matrix from the global to the local system. The generalized strains of the crack are denoted by $\boldsymbol{\epsilon}_{cr}$, and they are the equivalent of the jump vector, i.e. $\boldsymbol{\epsilon}_{cr} = [\![\mathbf{u}]\!]$. Hence, the transformation matrix $\mathbf{T}_{cr}$ may be seen as a strain distribution matrix of the crack, $\mathbf{B}_{cr}$, and we may write

$$\boldsymbol{\epsilon}_{cr} = \mathbf{B}_{cr} \mathbf{V}_d \tag{6}$$

which is the approximation of the generalized strains in the crack.

3. Physics and statics

3.1. Total quantities

The un-cracked material is assumed to be linear elastic and according to the Voigt notation the constitutive equation may be written in the form

$$\boldsymbol{\sigma} = \mathbf{D}\boldsymbol{\epsilon} \tag{7}$$

where $\mathbf{D}$ is the appropriate constitutive matrix for a disk. Since $\boldsymbol{\epsilon}$ by the choice of shape functions is the same on both sides of the discontinuity line, so is $\boldsymbol{\sigma}$, and stress compatibility in this respect is achieved inherently.

A crack is formed in the element when the first principal stress exceeds the uniaxial tensile strength of the material. For the crack we assume some relationship between the bridging stress vector and the crack opening vector, and we may write this in the general form

$$\boldsymbol{\sigma}_{cr} = \left\{ \begin{array}{c} \sigma_n(\boldsymbol{\epsilon}_{cr}) \\ \tau_{ns}(\boldsymbol{\epsilon}_{cr}) \end{array} \right\} \tag{8}$$

where σ_n is the normal bridging stress and τ_{ns} is the shear carried across the crack due to sliding friction.

Full stress compatibility is achieved by demanding the traction on the crack faces to equal the bridging stresses. Due to the above mentioned stress compatibility we need only look at the traction on one of the crack faces. The traction $\mathbf{t}^-$ on the crack face with $\mathbf{n} = [n_1 \ n_2]^T$ as outward normal is related to Ω_e^- and given by

$$\mathbf{t}^- = \mathbf{m}\boldsymbol{\sigma}\,, \qquad \mathbf{m} = \left[\begin{array}{ccc} n_1 & 0 & n_2 \\ 0 & n_2 & n_1 \end{array} \right] \tag{9}$$

The compatibility requirement may then be expressed as

$$\boldsymbol{\sigma}_{cr} = \mathbf{T}_{cr}\mathbf{t}^- \tag{10}$$

which may be expanded into the following

$$\boldsymbol{\sigma}_{cr}\left(\mathbf{V}_d\right) = \mathbf{T}_{cr}\mathbf{m}\mathbf{D}\left[\mathbf{B}_c\mathbf{V}_c + \mathbf{B}_d\mathbf{V}_d\right] \tag{11}$$

The nature of this equation depends on (8), and in general it is nonlinear in $\mathbf{V}_d$. However, it may be solved for $\mathbf{V}_d$ at the element level, thus allowing for the elimination of the d.o.f.'s describing the discontinuity. In general this involves an iteration at the element level and at every deformation state. In the case where (8) is given as multi-linear expressions, rather than general non-linear expressions, Equation (11) becomes a linear relation between $\mathbf{V}_c$ and $\mathbf{V}_d$ from which $\mathbf{V}_d$ is readily obtained as a function of $\mathbf{V}_c$.

3.2. Increments

Differentiation of (11) provides a relationship between the increments $\mathrm{d}\mathbf{V}_d$ and $\mathrm{d}\mathbf{V}_c$:

$$\frac{\partial \boldsymbol{\sigma}_{cr}}{\partial \boldsymbol{\epsilon}_{cr}} \frac{\partial \boldsymbol{\epsilon}_{cr}}{\partial \mathbf{V}_d} \, \mathrm{d}\mathbf{V}_d = \mathbf{T}_{cr}\mathbf{m}\mathbf{D} \left[\mathbf{B}_c \, \mathrm{d}\mathbf{V}_c + \mathbf{B}_d \, \mathrm{d}\mathbf{V}_d\right] \tag{12}$$

Introducing $\mathbf{D}_{cr}$ as the generalized tangential stiffness of the crack bridging we may write

$$\mathbf{D}_{cr} = \frac{\partial \boldsymbol{\sigma}_{cr}}{\partial \boldsymbol{\epsilon}_{cr}} \tag{13}$$

where $\mathbf{D}_{cr} = \mathbf{D}_{cr}(\mathbf{V}_d)$ is a function of the crack opening. By realizing that $\partial \boldsymbol{\epsilon}_{cr} / \partial \mathbf{V}_d = \mathbf{B}_{cr}$ we may isolate $\mathrm{d}\mathbf{V}_d$ from (12), furnishing

$$\mathrm{d}\mathbf{V}_d = \mathbf{Z} \, \mathrm{d}\mathbf{V}_c \tag{14}$$

where

$$\mathbf{Z} = \left[\mathbf{D}_{cr}\mathbf{B}_{cr} - \mathbf{T}_{cr}\mathbf{m}\mathbf{D}\mathbf{B}_d\right]^{-1} \mathbf{T}_{cr}\mathbf{m}\mathbf{D}\mathbf{B}_c \tag{15}$$

It should be emphasized that $\mathbf{Z}$ is a function of $\mathbf{V}_d$. Hence, by iteration the discontinuity increments may be eliminated at the element level, given the state of deformation.

4. Variational FEM formulations

The inherent lack of inter-element conformity previously mentioned is not accounted for in the variational formulation. Thus, only the local element contributions to the global behavior are considered and the contributions from the inter-element discontinuities are discarded. The justification for this is that the incompatibilities will decrease with mesh refinement, due to the decrease of the inter-element jump in crack opening. Further, the inter-element discontinuities are restrained through the interaction between neighboring elements.

Consider an element over the domain Ω_e with the boundary Γ_e and a domain load denoted by $\mathbf{f}$. Some part of the element boundary, Γ_{et}, may be part of the loaded boundary on which the prescribed traction $\bar{\mathbf{t}}$ acts. The element is assumed to hold a straight crack dividing the domain into two sub-domains Ω_e^- and Ω_e^+, and the intersecting crack line is denoted by S_e. The contribution to the internal virtual work from a cracked element, δW_e^I, may then be stated as

$$\delta W_e^I = \int_{\Omega_e} \delta \boldsymbol{\epsilon}^T \boldsymbol{\sigma} \, \mathrm{d}\Omega + \int_{S_e} \delta \boldsymbol{\epsilon}_{cr}^T \boldsymbol{\sigma}_{cr} \, \mathrm{d}S \tag{16}$$

and the contribution to the external virtual work, δW_e^E, may be stated as

$$\delta W_e^E = \int_{\Omega_e} \delta \mathbf{u}^T \mathbf{f} \, \mathrm{d}\Omega + \int_{\Gamma_{et}} \delta \mathbf{u}^T \bar{\mathbf{t}} \, \mathrm{d}\Gamma \tag{17}$$

where the prefix δ denotes the variation of the subsequent field. Note that, due to the special characteristics of the discontinuous shape function, integrals over the element domain are not affected by the discontinuity line; except in the case of body forces where the evaluation requires a subdivision of the domain. Introducing the approximations given previously we arrive at the following discrete form

$$\delta W_e^I = \left[\begin{array}{cc} \delta \mathbf{V}_c^T & \delta \mathbf{V}_d^T \end{array} \right] \left[\int_{\Omega_e} \mathbf{B}^T \mathbf{D} \mathbf{B} \, \mathrm{d}\Omega \right] \left\{ \begin{array}{c} \mathbf{V}_c \\ \mathbf{V}_d \end{array} \right\} + \delta \mathbf{V}_d^T \int_{S_e} \mathbf{B}_{cr}^T \boldsymbol{\sigma}_{cr} \, \mathrm{d}S \tag{18}$$

At any state of deformation we may calculate $\mathbf{V}_d$ as a function of $\mathbf{V}_c$ by iteratively solving (11), and stresses in the continuum as well as in the crack may be established. Also, at any state of deformation we may, analogously to (14), establish a relation between the variations given by $\delta \mathbf{V}_d = \mathbf{Z} \, \delta \mathbf{V}_c$, keeping in mind that $\mathbf{Z}$ is a function of $\mathbf{V}_d$. Then by utilizing (4) and (7) we may rewrite (18) in the form

$$\delta W_e^I = \delta \mathbf{V}_c^T \left[\left[\int_{\Omega_e} \left[\begin{array}{cc} \mathbf{I} & \mathbf{Z}^T \end{array} \right] \mathbf{B}^T \boldsymbol{\sigma} \, \mathrm{d}\Omega \right] + \int_{S_e} \mathbf{Z}^T \mathbf{B}_{cr}^T \boldsymbol{\sigma}_{cr} \, \mathrm{d}S \right] \tag{19}$$

where $\mathbf{I}$ has been introduced as the identity matrix.

In (19) the terms embraced by the outer pair of brackets constitute the element contribution to the internal nodal force vector, $\mathbf{Q}$. At the global level the virtual work equation furnishes the discrete equilibrium equations:

$$\mathbf{Q}(\mathbf{V}) = \mathbf{R} \tag{20}$$

where $\mathbf{V}$ is the global d.o.f. vector representing the continuous element d.o.f.'s, $\mathbf{V}_c$, only; $\mathbf{R}$ is the global load vector. Equation (20) is a set of nonlinear equations which must be solved iteratively applying a linear incremental relation.

A linear relation between increments of state variables may be established through differentiation of the virtual work equation. The differential form of the internal virtual work is given by

$$\mathrm{d}\delta W_e^I = \int_{\Omega_e} \delta \boldsymbol{\epsilon}^T \mathrm{d}\boldsymbol{\sigma} \, \mathrm{d}\Omega + \int_{S_e} \delta \boldsymbol{\epsilon}_{cr}^T \mathrm{d}\boldsymbol{\sigma}_{cr} \, \mathrm{d}S \tag{21}$$

and the discrete form reads

$$\mathrm{d}\delta W_e^I = \left[\begin{array}{cc} \delta\mathbf{V}_c^T & \delta\mathbf{V}_d^T \end{array}\right] \left[\int_{\Omega_e} \mathbf{B}^T\mathbf{D}\mathbf{B}\,\mathrm{d}\Omega\right] \left\{\begin{array}{c} \mathrm{d}\mathbf{V}_c \\ \mathrm{d}\mathbf{V}_d \end{array}\right\} + \delta\mathbf{V}_d^T \left[\int_{S_e} \mathbf{B}_{cr}^T\mathbf{D}_{cr}\mathbf{B}_{cr}\,\mathrm{d}S\right] \mathrm{d}\mathbf{V}_d \tag{22}$$

Again, at any state of deformation we may calculate $\mathbf{V}_d$ as a function of $\mathbf{V}_c$ by iteratively solving (11); and further, by utilizing the linear relation between differentials $\mathrm{d}\mathbf{V}_d = \mathbf{Z}\,\mathrm{d}\mathbf{V}_c$ and between variations $\delta\mathbf{V}_d = \mathbf{Z}\,\delta\mathbf{V}_c$ we arrive at

$$\mathrm{d}\delta W_e^I = \delta\mathbf{V}_c^T \left[\int_{\Omega_e} \left[\begin{array}{cc} \mathbf{I} & \mathbf{Z}^T \end{array}\right] \mathbf{B}^T\mathbf{D}\mathbf{B} \left[\begin{array}{c} \mathbf{I} \\ \mathbf{Z} \end{array}\right] \mathrm{d}\Omega + \int_{S_e} \mathbf{Z}^T\mathbf{B}_{cr}^T\mathbf{D}_{cr}\mathbf{B}_{cr}\mathbf{Z}\,\mathrm{d}S\right] \mathrm{d}\mathbf{V}_c \tag{23}$$

The terms within the outer brackets constitute the element contribution to the global tangent stiffness matrix, $\mathbf{K}_t$, which furnishes the relation between increments of the load and deformation vectors:

$$\mathbf{K}_t\,\mathrm{d}\mathbf{V} = \mathrm{d}\mathbf{R} \tag{24}$$

The element is based on the CST, however, it allows for the formation of a displacement discontinuity. Thus, we have named the element "dCST". The dCST has three nodes and six d.o.f.'s, two at each node describing the displacement vector. The actual value of the discontinuity vector is calculated at the element level and no global d.o.f.'s are needed to represent these vector elements. A crack is formed if the principal stress in the element exceeds the uniaxial tensile strength, and the normal to the discontinuity line is parallel to the principal stress vector at initiation of the crack. If a neighboring element is in the cracked state, the crack in the actual element is forced to connect to the neighboring crack; otherwise it is forced to pass through the center of the element or some other predefined point. The nonlinear equilibrium equations may be solved by standard FEM procedures.

5. Benchmark applications

The performance of the dCST element is demonstrated through three application examples, which have become standard benchmark tests for cohesive crack elements. In all of these tests fracture propagation is dominated

by Mode I behavior, thus the mixed mode capabilities of the element are not challenged. The mixed mode action is outside the scope of this paper, and it would require the implementation of a proper mixed mode material model to allow for such tests of the dCST element. Therefore, at this point we have implemented an elastic resistance against the mutual sliding of the cracked faces, i.e. τ_{ns} is modeled as a linear function of u_s.

The solution strategy followed in these examples is the same and based on the following concept: First a linear analysis determines the first crack situation and a crack is initiated emanating from the midpoint of an element side. The direction of the crack path is determined from the principal stress direction. The next equilibrium point is established as the situation corresponding to the load at which a crack in the neighboring element is initiated. The path of the new crack is linked to the previous crack path, thus only the penetration of one single crack is modeled. The last step is repeated until breakdown of the solution. If the softening curve of the material is approximated by a multi-linear function, this approach is very efficient, since the tangent stiffness matrix will then be stepwise constant.

5.1. Center cracked sheet

The first benchmark test models the cohesive crack growth in an infinite sheet with an initial stress free slit subject to a uniaxial far field stress, σ_{ff}. The slit is perpendicular to the stress direction and measures $2a_0$. A semi-analytical solution to this problem has been presented in [23], which we will verify our results against.

The element model approximation of the infinite sheet measures 1200 by 1000 mm and the slit size is given by $a_0 = 2$ mm, as depicted in Figure 2. These dimensions amply fulfill the infinity requirements. The cohesive properties of a material crack are given as a bilinear curve, also shown in Figure 2, and the material properties are listed in Table 1. These properties are characteristic of a concrete mortar.

Table 1: Material properties for center cracked sheet.

$f_t = 2.83$	[MPa],	$a_1 = 156.0$	[mm^{-1}]
$E = 31.0$	[GPa],	$a_2 = 9.70$	[mm^{-1}]
$\nu = 0.20$	[-],	$b_1 = 0.24$	[-]

Two mesh densities have been used to model the sheet, see Figure 3. The meshes model the right half of the sheet and are unstructured apart from a horizontal strip of regularly shaped elements to the right of the slit. The slit itself is modeled by stress free elements. In the coarser mesh the element side length is 4 mm, whereas it is 2 mm in the finer mesh. In this application the crack path has been fixed, such that it remains horizontal throughout the loading history. This has been done to demonstrate the element performance under pure Mode I conditions, leaving out the effects that would arise from a winding crack path which is inevitable if the crack was to find its own way.

Results are presented in Figure 4 where the far-field stress is plotted versus the crack length, a, which holds the initial stress free part of length a_0. Thus, the length of the material crack is given by $a - a_0$. The dCST results are shown together with the semi-analytical reference solution, which is shown as a solid curve. All results are close to the reference curve, although the fine mesh shows the best performance both in terms of accuracy and in terms of ability to track large crack openings. Where the results of the coarse mesh stop at a crack length of approximately 46 mm, the results of the fine mesh continue until a crack length of 80 mm. These remarkable results are achieved for regularly shaped elements traversed by a crack through the midpoint of pairs of elements. They show that the basics of the element are trustworthy, however, under constrained use. In the next two applications the restrictions imposed here on the location of the crack are gradually released.

5.2. Three point bending beam

This second benchmark test models the cohesive crack growth in a beam with a notch subject to three point bending, as shown in Figure 5. The 4 mm wide notch is placed at the midsection and is perpendicular to the beam axis, the depth of it corresponds to one sixth of the beam height. The material parameters are listed in Table 2. These properties are characteristic of a normal strength concrete and the tension softening relationship is assumed to be linear with values corresponding to a fracture energy of 160 N/m.

Table 2: Material properties for three point bending beam.

$f_t = 3.50$	[MPa],	$\nu = 0.20$	[-]
$E = 37.4$	[GPa],	$a_1 = 10.938$	[mm^{-1}]

The notched beam was meshed with an un-structured mesh (USM) with three different densities as show in Figure 5. The USM-number signifies the number of characteristic element heights over the ligament at the notched cross-section. Note that the geometry of the notch was modeled exactly. In this case, however, the crack path was controlled such that it extended from the notch into the beam perpendicular to the beam axis. Thus, the elements were not traversed by the crack in a systematic manner as it was the case in the previous example.

Figure 6 presents the results of the simulations with the dCST element in different mesh densities. The results are compared with a reference simulation with the commercially available finite element programme DIANA. This simulation by [11] was considered to be sufficiently accurate, and it was made by applying 48 standard interface elements with a quadratic displacement interpolation along the crack path, predefined to follow the midsection of the beam. The midpoint deflection is measured as the difference between downward deformation of the midsection and the downward deformation of a point at mean height in the beam end above the support. Hereby the local deformations due to concentrated stress at the support are disregarded.

All results are good predictions of the beam behavior as given by the reference curve, although the peak load is captured better, the finer the mesh is. Especially, on the descending part of the curve the coarse mesh deviates some from the reference simulation. All three meshes demonstrate good ability to follow the load-displacement curve, however, when only two or three elements are still un-cracked the solution is no longer feasible.

The results presented here were achieved for the un-structured meshes but under crack path control. They show that the element handles the formation of cracks at arbitrary locations in the element adequately, however, under the restriction that the overall crack path has been predefined. In the next application no restrictions regarding the crack path are imposed.

5.3. Four point shear beam

The third and final benchmark test models the cohesive crack growth in a beam with a notch subject to four point shear loading, as shown in Figure 7. The 4 mm wide notch is cut from the top face at the midsection and is perpendicular to the beam axis, the depth of it corresponds to one fifth of the beam height. The material parameters are listed in Table 3 in accordance with the experimental data reported in [24]. The tension softening relationship is assumed to be linear with values corresponding to a fracture energy

of 145 N/m.

Table 3: Material properties for four point shear beam.

$f_t = 2.40$	[MPa],	$\nu = 0.10$	[-]
$E = 28.0$	[GPa],	$a_1 = 8.276$	[mm^{-1}]

Figure 8 presents the results of the simulations with the dCST element in different mesh densities. The results are compared with the experimental observations reported in [24] and with the simulations presented in [12] obtained with the higher order XFEM LST element which may be partly cracked (later referred to as the reference curve). Deflections are given at Points *I* and *II* in the midplane of the beam under the loading points, see Figure 7. The deflections are plotted against the proportional part of the total load, P, transmitted at each loading point, i.e. $9P/10$ and $P/10$, respectively.

Results for the two finer meshes give good predictions for the beam behavior as compared with the reference curve. Although comparison with the experimental curve is less convincing, the model does capture the characteristic features of the test. The results for the coarse mesh are less precise and convergence was not obtained for large deflections (beyond the peak load). It should be emphasized that the results presented here were achieved for unstructured meshes and without restrictions on the crack path. In other words it is demonstrated that the element handles the free formation of cracks at arbitrary locations in the element adequately.

6. Conclusion

In this paper a simple element for modeling cohesive fracture processes in quasi-brittle materials has been developed and tested. The element is based on the CST element and the crack is embedded in the element, i.e. extra d.o.f.'s controlling the crack opening are eliminated at the element level. The cracked element is stress-compatible in the sense that stresses are continuous across the crack, i.e. the traction on the crack faces balance each other and they are equal to the bridging stresses. A special shape function is introduced to allow for the discontinuous displacements. The normal and tangential discontinuities must both be constant in each element in order not

to eradicate the required stress compatibility. The element distinguishes itself from other embedded elements by the exact enforcement of stress continuity in a strong form. The element formulation is based on a standard variational principle of virtual work involving only variational deformation fields, i.e. there has been no need to resort to more advanced multi-field formulations, such as the assumed strain method.

The good performance of the element has been demonstrated through the comparison with three benchmark tests in which a single crack is propagated. First, the center cracked sheet in uni-axial tension was modeled, and it was shown how the element performs appropriately when the element mesh is regular and the crack path is controlled. Then, the three-point bending test was modeled, and the element mesh was allowed to be irregular, however, still with a controlled crack path. Again the element performed well. Finally, the four-point shear beam test was modeled, and the element mesh was allowed to be irregular and at the same time the crack path was unrestricted. Good result were obtained in this case, too.

References

[1] Hillerborg A, Moder M, Peterson PE. Analysis of crack formation and crack growth in concrete by means of fracture mechanics and finite elements. Cement Concrete Research 1976; 6:773–782.

[2] Belytschko T, Black T. Elastic crack growth in finite elements with minimal remeshing. International Journal for Numerical Methods in Engineering 1999; 45(5):601–620.

[3] Moës N, Dolbow J, Belytschko T. A finite element method for crack growth without remeshing. International Journal for Numerical Methods in Engineering 1999; 46(1):131–150.

[4] Rabczuk T, Bordas S, Zi G. On three-dimensional modelling of crack growth using partition of unity methods. Computers and Structures 2010; 88: 1391-1411

[5] Jirásek M, Belytschko T. Computational resolution of strong discontinuities. In Proceedings of Fifth World Congress on Computational Mechanics, Mang HA, Rammerstorfer FG, Eberhardsteiner J (Eds.), 2002

[6] Wells GN, Sluys LJ. A new method for modelling cohesive cracks using finite elements. International Journal for Numerical Methods in Engineering 2001; 50(12):2667–2682.

[7] Moës N, Belytschko T. Extended finite element method for cohesive crack growth. Engineering Fracture Mechanics 2002; 69(7):813–833.

[8] Asferg JL, Poulsen PN, Nielsen LO. A direct XFEM formulation for modeling cohesive crack growth in concrete. Computers and Concrete 2007; 4(2):83–100.

[9] Areias PMA, Belytschko T. Analysis of three-dimensional crack initiation and propagation using the extended finite element method. International Journal for Numerical Methods in Engineering 2005; 63:760-788.

[10] Zi G, Belytschko T. New crack-tip elements for XFEM and applications to cohesive cracks. International Journal for Numerical Methods in Engineering 2003; 57(15):2221–2240.

[11] Asferg JL, Poulsen PN, Nielsen LO. A consistent partly cracked XFEM element for cohesive crack growth. International Journal for Numerical Methods in Engineering 2007; 72(4):464–485.

[12] Mougaard JF, Poulsen PN, Nielsen LO. A partly and fully cracked triangular XFEM element for modeling cohesive fracture. International Journal for Numerical Methods in Engineering 2010; 85(13):1667–1686.

[13] Karihaloo BL, Xiao Q-Z. Accurate simulation of mixed-mode cohesive crack propagation in quasi-brittle structures using exact asymptotic fields in XFEM: An overview Journal of Mechanics of Materials and Structures 2011; 6(1-4)(SI):267–276

[14] Oliver J, Huespe AE, Sánchez PJ A comparative study on finite elements for capturing strong discontinuities: E-FEM vs X-FEM Computer Methods in Applied Mechanics and Engineering 2006; 195:4732-4752.

[15] Jirásek M, Belytschko T. Computational resolution of strong discontinuities. In H.A. Mang, F.G. Rammerstorfer, J. Eberhardsteiner (Eds.) Proceedings of Fifth World Congress on Computational Mechanics, Vienna, Austria 2002;

[16] Jirásek M. Comparative study on finite elements with embedded discontinuities. Computer Methods in Applied Mechanics and Engineering 2000; 188(1-3):307–330.

[17] Oliver J. Modelling strong discontinuities in solid mechanics via strain softening constitutive equations. Part 2: Numerical simulation. International Journal for Numerical Methods in Engineering 1996; 39:3601–3623.

[18] Feist C, Hofstetter G. An embedded strong discontinuity model for cracking of plain concrete Computer Methods in Applied Mechanics and Engineering 2006; 195:7115-7138.

[19] Linder C, Armero F. Finite elements with embedded strong discontinuities for the modeling of failure in solids International Journal for Numerical Methods in Engineering 2007; 72:1391–1433.

[20] Simo JC, Rifai S. A class of mixed assumed strain methods and the method of incompatible modes. International Journal for Numerical Methods in Engineering 1990; 29:1595–1638.

[21] Dvorkin EN, Cuitio AM, Gioia G. Finite elements with displacement interpolated embedded localization lines insensitive to mesh size and distortions. International Journal for Numerical Methods in Engineering 1990; 30:541–564.

[22] Sancho JM, Planas J, Cedón DA, Reyes E, Gálvez JC. An embedded crack model for finite element analysis of concrete fracture. Engineering Fracture Mechanics 2007; 74:75–86.

[23] Stang H, Olesen JF, Poulsen PN, Dick-Nielsen L. On the application of cohesive crack modeling in cementitious materials. Materials and Structures 2007; 40(4):365–374.

[24] Carpinteri A, Valente S, Ferrara G, Melchiorri G. Is mode II fracture energy a real material property?. Computers and Concrete 1993; 48(3):397–413.

List of Figures

List of Tables

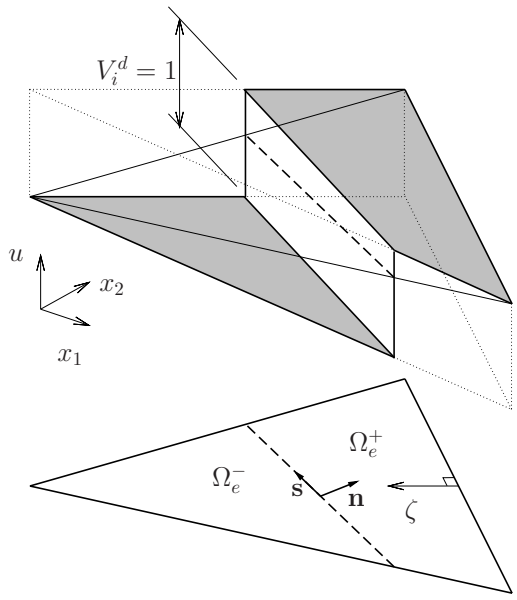

Figure 1: Discontinuous shape function. Element sub-domains, area coordinate and crack coordinate system definitions.

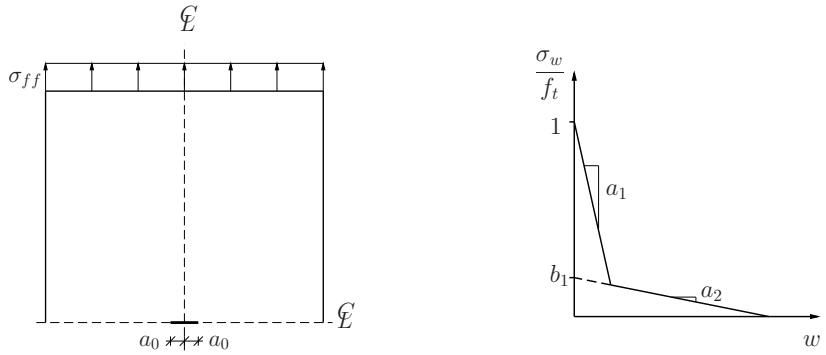

Figure 2: (a) Top symmetric part of a center cracked sheet with a stress free pre-crack. (b) Bilinear tension softening curve.

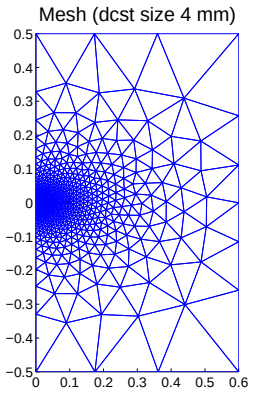

(a) Coordinates in m.

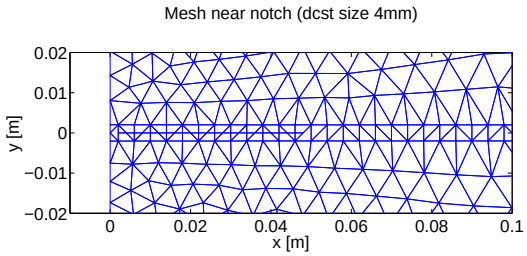

(b) Crack path.

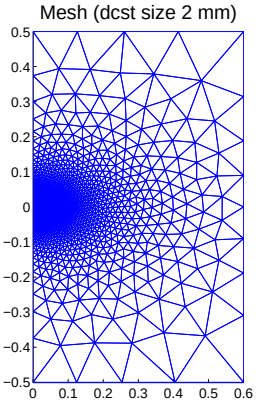

(c) Coordinates in m.

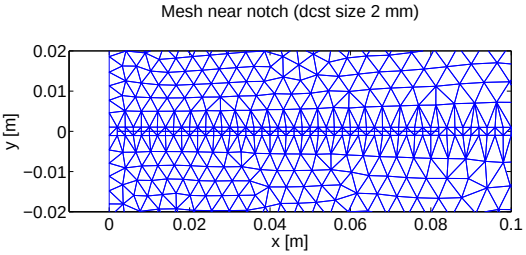

(d) Crack path.

Figure 3: Meshes for right symmetric half of center cracked sheet. Regular elements at horizontal symmetry line, (a)-(b): size 4 mm, (c)-(d): size 2 mm. Crack path shown at final load step.

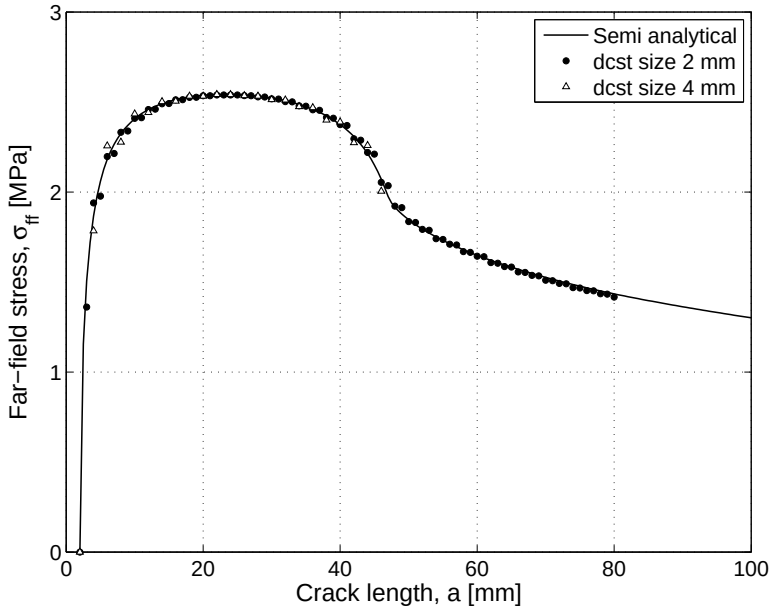

Figure 4: Center cracked sheet. Far-field stress versus the length of the crack. Legend: dcst = present element, size # mm = size of cracked elements.

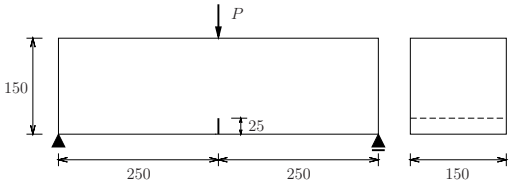

(a) Geometry, load and support of a beam with a 25 mm deep and 4 mm wide notch.

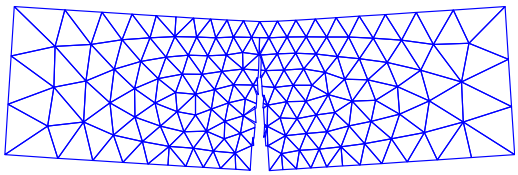

(b) USM 7: 259 elements.

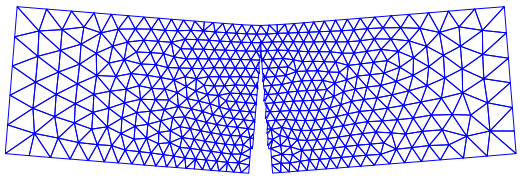

(c) USM 14: 861 elements.

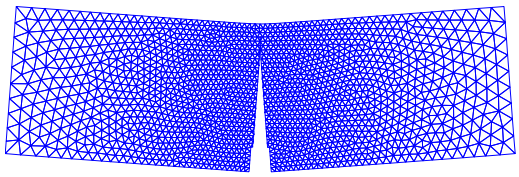

(d) USM 21: 3348 elements

Figure 5: Specifications and meshes for three-point bending beams. Deformed state shown at final load step scaled by a factor of 100. Legend: USM # = unstructured mesh with # elements over the height.

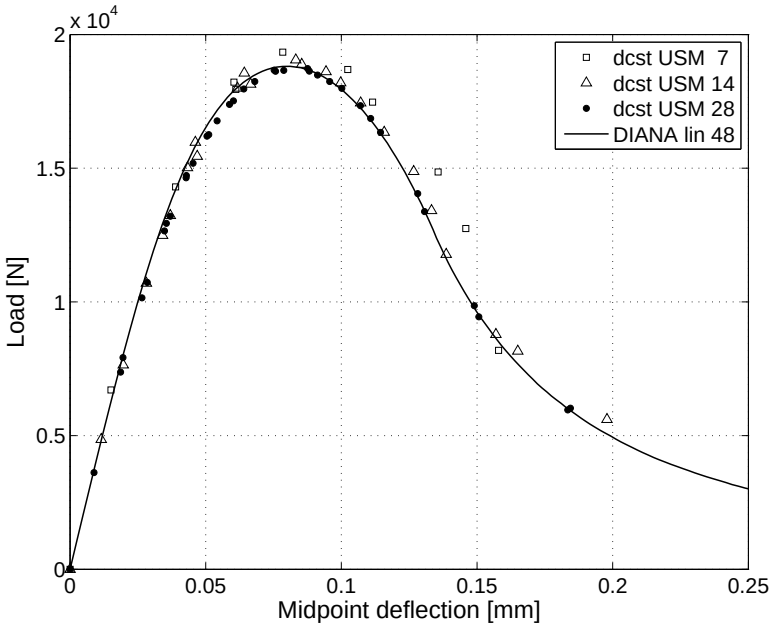

Figure 6: Three point bending test. Load versus deflection. Legend: dcst = present element, USM # = unstructured mesh with # elements over the height, DIANA lin 48 = DIANA interface model with 48 elements over the height.

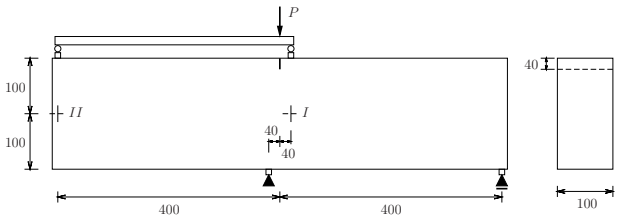

(a) Geometry, load and support of beam with 40 mm notch and 20 mm load platens.

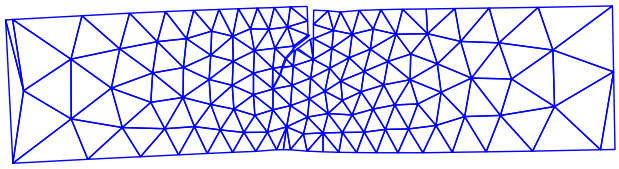

(b) USM 6: 861 elements.

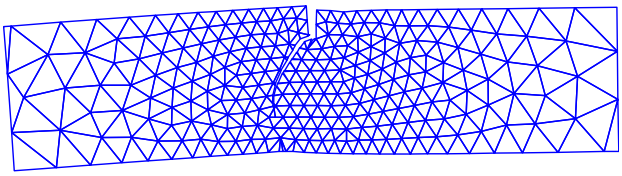

(c) USM 10: 493 elements

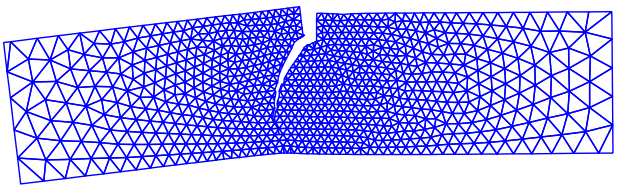

(d) USM 18: 3348 elements

Figure 7: Specifications and meshes for three-point bending beams. Deformed state shown at final load step scaled by a factor of 100.

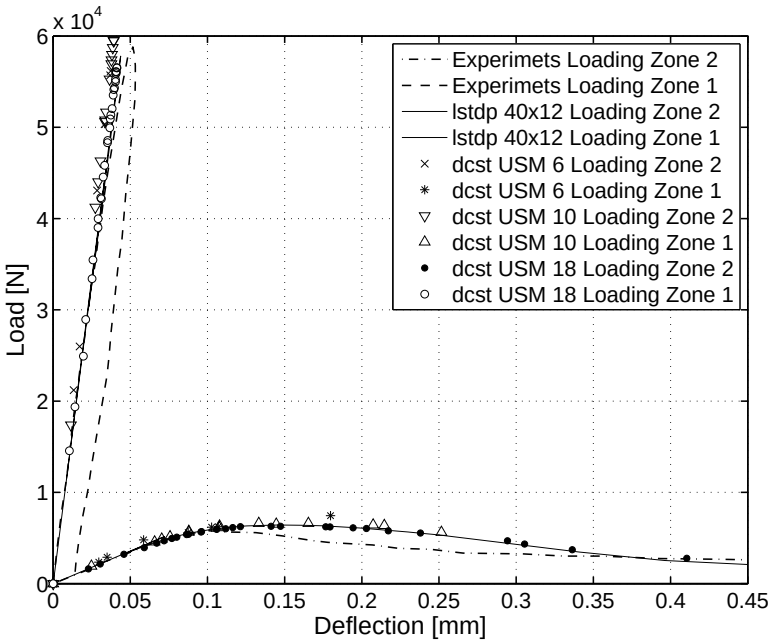

Figure 8: Four point shear test. Proportional part of load versus deflection at points I and II. Legend: 'lstdp' refers to results from [12]